Detection of metallic cylindrical inclusions by thermoelectric coupling

H. Carreon [a] and J.L. González-Carrasco[b]
[a]*Instituto de Investigaciones Metalúrgicas (UMSNH-IIM) Ciudad Universitaria, Morelia, Mexico,*
tel: + 011-52-443-316-7414
e-mail: hcarreon@umich.mx
[b]*Centro Nacional de Investigaciones Metalúrgicas (CENIM-CSIC),*
Avda. Gregorio del Amo 8, E28040 Madrid, España.

Recibido el 1 de febrero de 2012; aceptado el 29 de mayo de 2012

In this paper, we present a technique that can give information on surface metallic inclusions embedded in a host material, *i.e.* by the magnetic sensing of local thermoelectric currents produced when a temperature gradient is established in the material. These thermoelectric currents generate flux magnetic densities that are detected by a highly sensitive magnetometer. A comparison between reported analytical results with experimental data of the magnetic field produced by thermoelectric currents around surface-breaking cylindrical tin inclusions in copper under external thermal excitation for different lift-off distances between the sensor and the surface of the specimen is presented. The diameter of the inclusions varied from 4.76 to 12.7 mm at different lift-off distance magnetometer probe and the specimen 1 to 8 mm respetively. A fairly modest 1.46°C/cm temperature gradient in the specimen produced magnetic flux densities ranging from 60 to 1460 nT.

Keywords: Thermoelectric measurements; magnetic flux density; cylindrical inclusions; magnetometer.

PACS: 85.80.Fi; 85.70.Ag; 85.75.Ss; 81.05.Bx; 85.70.Ex

1. Introduction

Essentially all existing thermoelectric techniques are based on the well-know Seebeck effect that is used in thermocouples to measure temperature at the junction of two different conductors. These conventional techniques are solely sensitive to intrinsic material variations regardless of the shape and surface quality of the specimen to be inspected. However, they require a very good metallic contact between the specimen and the reference electrode; therefore the detectability of small material variations and imperfections is limited by the presence of the imperfect contact. On the other hand, we consider an alternative non contacting thermoelectric technique that uses the surrounding intact material as the reference electrode; thus provides perfect interface between the region to be tested and the surrounding material. This technique has the possibility to detect surface and subsurface metallic inclusions, by magnetic sensing [1-3]. The idea is to sense the weak thermoelectric currents around inclusions and other types of inhomogeneities when the specimen to be tested is subjected to directional heating or cooling by using high-sensitivity magnetic sensor. A schematic diagram of the thermoelectric measurements process in the presence of material imperfections is shown in Fig. 1. For this case, an external heating or cooling is applied to the specimen to produce a temperature gradient in the region to be tested. This leads to that different points of the boundary between the host material and the imperfection will be at different temperatures, therefore also at different thermoelectric potentials. This will produce opposite thermoelectric currents inside and outside the imperfection. The thermoelectric currents form local loops that run in opposite directions on the opposite sides of the imperfection relative to the prevailing heat flux.

When the specimen is scanned with a sensitive magnetometer, such as a superconducting quantum interference device (SQUID), the magnetic field of these thermoelectric currents can be detected even when the imperfection is buried below the surface and the sensor is as far as a couple of centimeters from the specimen [4,5]. It should be mentioned that high-temperature superconductor (HTS) SQUID magnetometers and gradiometers operating at the temperature of liquid nitrogen are currently used for noncontact detection of weak magnetic fields in a number of applications. These include magnetocardiography for diagnosis of cardiac arrhythmia [6], nondestructive evaluation (NDE) for very deep eddy-current flaw detection [7], and detection of small ferrous inclusions in aircraft engine discs [8], and electromagnetic geological prospecting [9].

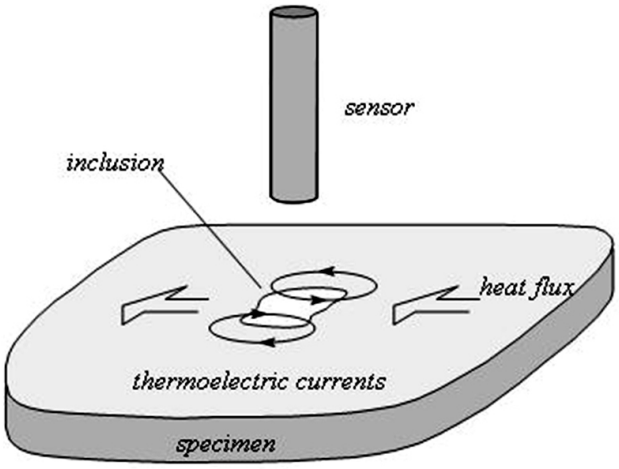

FIGURE 1. Schematic diagram of noncontacting thermoelectric detection of material imperfections by magnetic monitoring of thermoelectric currents.

In a published paper, an analytical model to predict the magnetic field produced by thermoelectric currents around surface-breaking cylindrical inclusions in a homogeneous host material under external thermal excitation was developed [10]. Although the best experimental tool for such studies is undoubtedly a SQUID-based magnetometer, we will use a fluxgate magnetometer to provide experimental evidence of the theoretical predictions through the example of surface-breaking cylindrical tin inclusions of varying diameter in a copper matrix at different lift off distances between the sensor and the surface specimen. First, we are going to present a brief review of the analytical model of Ref. 10, then we will proceed by describing the experimental procedure and, finally, discuss the experimental results and compare them to the analytical predictions.

2. Theoretical model

To simplify the analytical calculations, all spatial coordinates will be normalized to the radius of the cylindrical inclusion as $\xi = x/a$. The magnetic field can be also written in a normalized form as $\mathbf{H} = H_0\mathbf{F}(\xi)$. The estimation of the absolute strength of the magnetic field can be written as $H_0 = -a\nabla T\sigma(S' - S)\Gamma$ where a is the radius of the inclusion, ∇T is the externally induced temperature gradient, σ is the thermal conductivity of the host, $S_{SR} = S' - S$ is the relative thermoelectric power of the inclusion with respect to the host, while $\mathbf{F}(\xi)$ is a universal spatial distribution function for all cylindrical inclusions and Γ is the normalized contrast coefficient determined by the ratio between the electrical and thermal conductivities of the inclusion and the host (Γ=1/2 for similar materials). For the case of a cylindrical inclusion

$$\Gamma = \frac{2}{\left(1 + \frac{\sigma}{\sigma'}\right)\left(1 + \frac{\kappa'}{\kappa}\right)}\,. \tag{1}$$

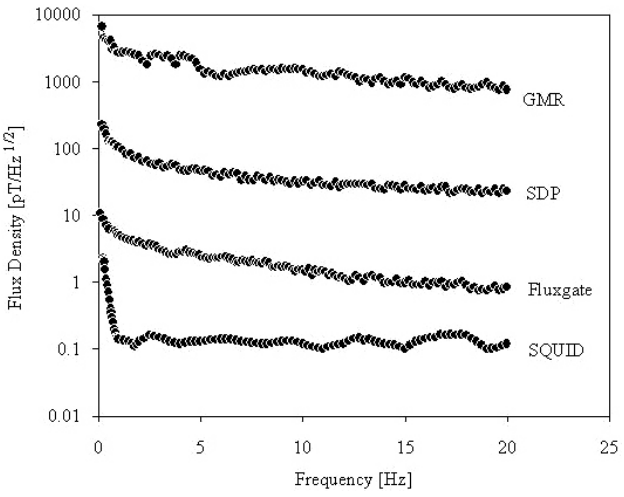

FIGURE 2. Typical noise spectra between 0.1 and 20 Hz for different magnetic sensors.

where κ is the thermal conductivity of the host and in order to differentiate between the properties of the two media, we designate those of the inclusion by a prime.

For a rough estimate of the strength of the magnetic field, let us assume that a modest $\nabla T = 1$ °C/cm temperature gradient is maintained in a 7075-T6 aluminum alloy specimen ($\sigma = 1.9 \times 10^7$ A/Vm) containing a cylindrical inclusion of $a = 1$ mm. The thermoelectric power of most metals is in the ± 10 μV/°C range, therefore we assume that the relative thermoelectric power of the inclusion with respect to the host is a modest $S_{SR} = -0.1$ μV/°C. With these parameters, we get or, in terms of magnetic flux density, $B_0 \approx 80$ nT. On the other hand, most structural metals have much lower electrical conductivity than aluminum. For example, in Ti-6Al-4V, the most popular aerospace titanium alloy, the electrical conductivity is $\sigma \approx 5.8 \times 10^5$ A/Vm, therefore the corresponding magnetic flux density is only $B_0 \approx 2.4$ nT.

Figure 2 shows the typical noise spectra between 0.1 and 20 Hz for various magnetic sensors currently available on the market such as Giant Magneto-Resistive (GMR) detectors, Spin Dependent Tunneling (SPD) detectors, fluxgates and, especially, Superconductive QUantum Interference Device (SQUID) magnetometers. Of course, the strength of the magnetic field to be detected greatly depends on the physical nature and dimensions of the imperfection, but for modest ($\approx 1 - 10$ °C/cm) temperature gradients the magnetic flux density is expected to be between 100 pT and 10 nT. The experimental results presented in this research work were obtained by a 3 axis magnetic field sensor Bartington Instruments Mag-03 fluxgate that has a noise-limited detection threshold of ≈2.5 pT/$\sqrt{\text{Hz}}$ over a bandwidth of 0.1 to 20 Hz. In comparison, the measured peak magnetic flux densities varied between 60 nT and 1650 nT, *i.e.*, the sensitivity of the fluxgate magnetometer was quite sufficient.

A schematic drawing of the normal component of the magnetic field $F_1(\xi_2, \xi_3)$ taken in planes parallel to the free surface at lift-off distances of ξ_1 = 0 and ξ_1 = 0.5 respectively for an inclusion with its center lying on the surface is shown in Fig 3. As it could be expected qualitatively from Fig. 1, the thermoelectric currents flow in opposite directions along two loops on the opposite sides of the inclusion relative to the direction of the heat flux, therefore the magnetic field is asymmetric with respect to this direction. The characteristic shape produced by the positive and negative peaks in the magnetic field distribution are very typical in noncontacting thermoelectric detection of inclusions and can be easily exploited by digital image processing and feature extraction techniques to increase the probability of detection for inclusions [11-12]. The larger the lift-off distance, the lower the peak magnetic field and the wider the field distribution. The latter can be quantitatively characterized by the lateral distance of the peaks from the center of the inclusion, which we are going to call the half-width of the bi-polar signature. Since the field distribution remains very similar regardless of the lift-off distance, it is reasonable to choose the two parameters, namely the peak magnetic field and the half-distance

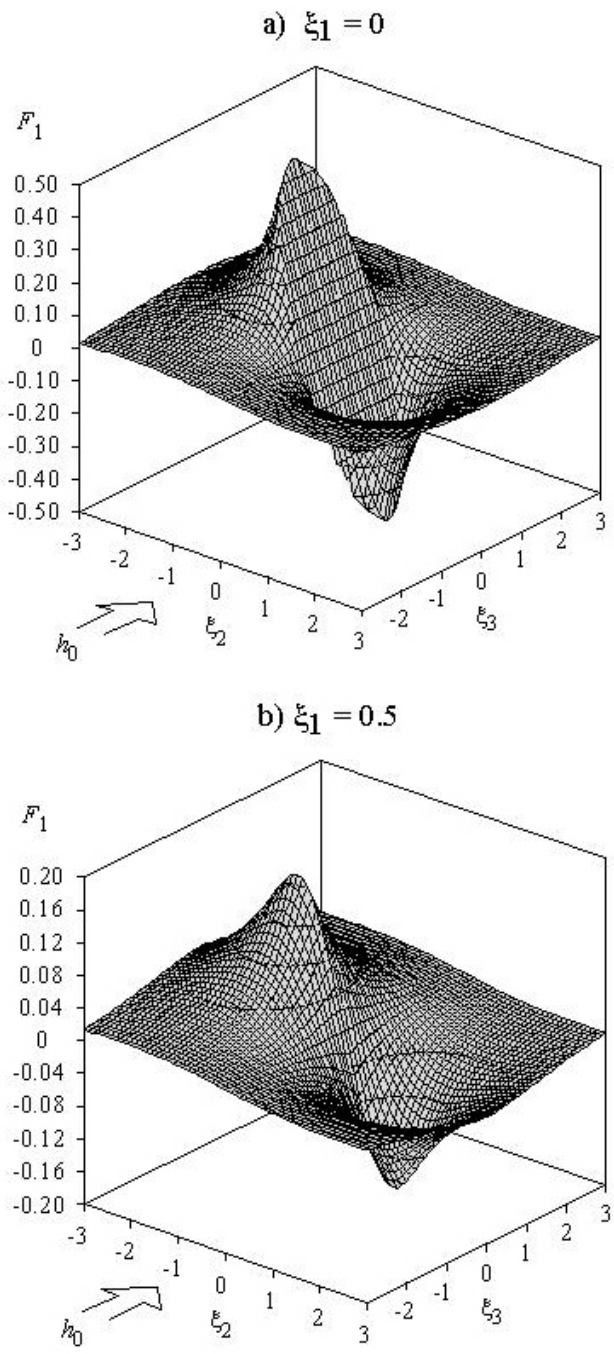

FIGURE 3. A schematic drawing of the normal component of the magnetic field taken in different planes parallel to the free surface at two lift-off distances for an inclusion with its center lying on the surface.

between the peaks, to qualitatively characterize the whole field distribution.

3. Experimental Method

In this section, we review some of the experimental results which demonstrate that the described analytical model capable of predicting the magnetic field produced by thermoelectric currents around cylindrical inclusions under external thermal excitation truthfully captures the main features of the thermoelectrically generated magnetic field and accurately predicts its magnitude over a wide range of inclusion sizes and lift-off distances. We prepared a series of cylindrical tin inclusions embedded in copper bars of 12.7×38.1×250 mm dimensions. First, we prepared the cylindrical holes by milling from the specimen surface, then we heated the specimens to approximately 300°C and filled the holes with molten tin, and finally milled the surface flat after the specimen has cooled down. The diameter of the artificial tin inclusions in the copper matrix varied from 4.76 to 12.7 mm and the center of each inclusion was at the level of the specimen surface. The distance between inclusions was approximately 30 mm to avoid interference between their individual magnetic fields. Both ends of the copper specimen were perforated by a series of holes and equipped with sealed heat exchangers to facilitate efficient heating and cooling and then mounted on a non-magnetic translation table for scanning. The physical properties of pure copper $\sigma = 59.7\times10^6$ A/Vm, κ =399 × VA/m°C, $S = 1.72 \times10^{-6}$ V/°C and tin $\sigma = 8.31\times10^6$ A/Vm, $\kappa = 62.4\times$ VA/m°C, $S = -1.73\times10^{-6}$ V/°C were used to make a quantitative comparison to the analytical predictions.

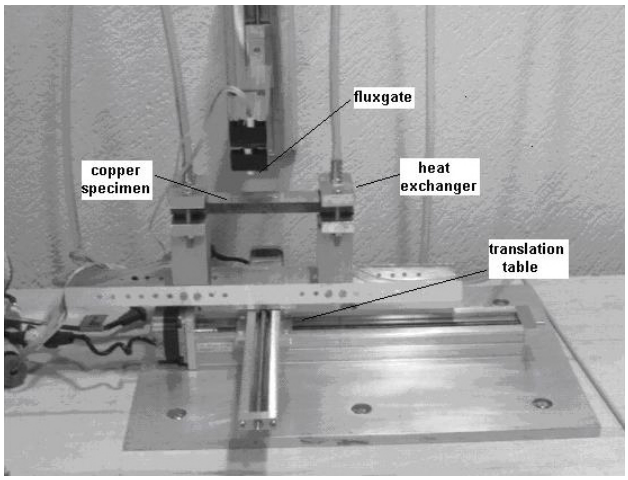

FIGURE 4. Experimental arrangement.

Figure 4 shows the experimental arrangement. The copper specimen was mounted and equipped by the heater exchangers to heat and cool it simultaneously by running water at temperature of ≈ 5°C and ≈ 40°C, respectively. All the assembly was mounted on a translation table for scanning. Since the temperature of the cold and hot water in the laboratory inevitably fluctuated by a couple degrees, the actual temperature difference between the ends of the bar was monitored during the magnetic flux density measurements. The temperature gradient was between 1.2°C/cm and 1.6°C/cm, which is more than enough to produce detectable magnetic signals in high-conductivity materials such copper and tin. The experimental data were always obtained as the difference between measurements taken at opposite heating directions. As it is indicated in Fig. 4, alternating the heating and cooling

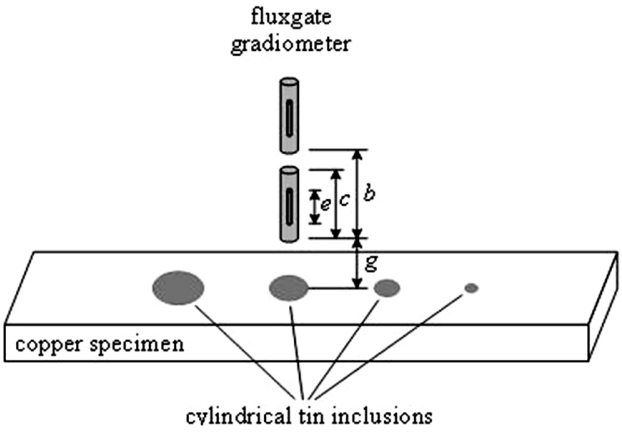

FIGURE 5. Parameters of the two sensing elements in a gradiometric configuration.

directions was achieved simply by changing the hot and cold water supplies connected to the heat exchangers and waiting a few minutes until steady-state conditions were reached.

The magnetic signals to be detected from the tin inclusions are generated in the close vicinity of the magnetometer therefore they exhibit strong gradients. Extraneous signals typically originate at larger distances from the magnetometer, therefore they exhibit relatively small gradients. In order to exploit this difference, we used only two sensing elements in a gradiometric configuration. The primary sensing element closer to the copper specimen get a much stronger signal from the inclusion than the secondary sensing element, while the two sensing elements exhibit essentially the same sensitivity for sources at large distances. The baseline distance (b in Fig. 5) was chosen to be 26 mm in our case. Further reduction of the baseline distance would improve the rejection of extraneous signals but would also reduce the sensitivity to the thermoelectric signals to be detected.

4. Experimental Results

In order to compare the magnetic signature produced by the thermoelectric currents around inclusions of specific geometries under external heating or cooling. Figure 6 shows examples of the two magnetic images obtained from a i) surface-breaking cylindrical tin inclusion and ii) a surface-breaking semi-spherical tin inclusion embbeded in a copper specimen respectively. Both magnetic images shows the characteristic bipolar lobes of the thermoelectric signal. The magnetic field distribution of the i) surface-breaking cylindrical tin inclusion is obviously very similar to that of the ii) surface-breaking semi-spherical tin inclusion [3], except that the bipolar lobes are more extended and rounded affected by the cylindrical inclusion shape. Also, the thermoelectric currents flow in opposite directions along two loops on the opposite sides of the inclusion depends on the heat flux direction as predicted by Fig. 1. These measured thermoelectric magnetic images were taken at g = 2 mm distance above the surface (see Fig. 5). This apparent lift-off distance is the actual gap

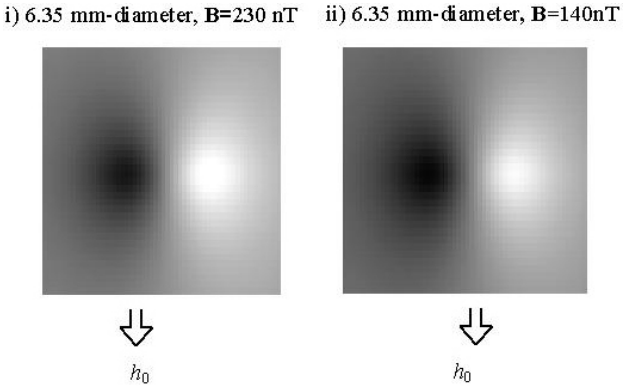

FIGURE 6. Comparison of magnetic signature between a i) a surface-breaking cylindrical tin inclusion and ii) a surface-breaking semi-spherical tin inclusion embbeded in a copper specimen.

between the tip of the magnetometer probe and the specimen. However, the sensing element of the fluxgate is an $e = 15$ mm long ferromagnetic rod of d = 2 mm diameter centered in a c = 25 mm long case. The geometric center of the fluxgate is approximately 12.5 mm below the tip of the case, *i.e.*, the 2 mm apparent lift-off corresponds to a much larger 14.5-mm actual lift-off distance. This approximation, however, will not be sufficient for the purposes of quantitative comparison to the analytical predictions, therefore we used the unknown effective depth of sensing element as a variable parameter. Our goal is to establish a crude approximation for the actually studied case of short cylindrical inclusions. Because we recognize that those predictions are limited to an infinity inclusion embedded in an infinite host.

Figure 7 compares the experimentally measured symbols) and theoretically predicted (semi-solid line) magnetic flux densities for the apparent lift-off distance between 1 and 8 mm for cylindrical inclusions of different diameters between 4.76 and 12.7 mm. The semi-solid lines represent the analytical predictions based on the material properties listed above. For each inclusion diameter and lift-off distance, the

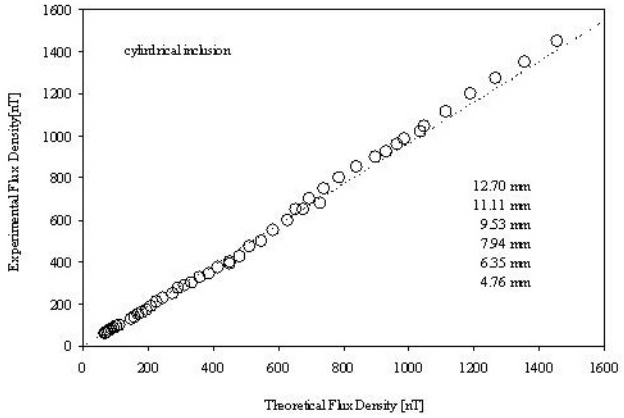

FIGURE 7. Comparison between the experimentally measured (symbols) and theoretically predicted (semi-solid line) peak-to-peak magnetic flux densities plotted as functions of the lift-off distance for surface-breaking cylindrical tin inclusions embedded in copper.

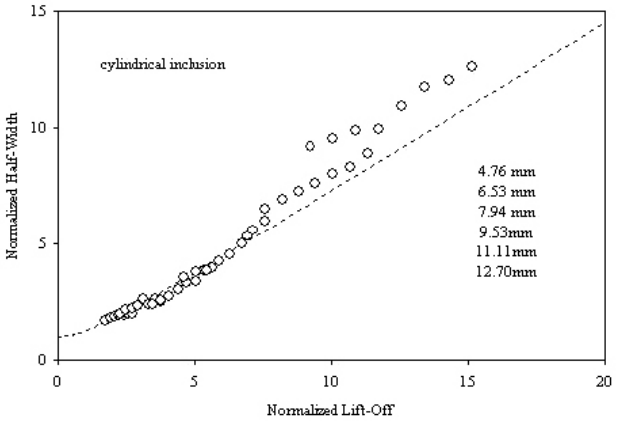

FIGURE 8. Theoretical predictions (semi-solid line) and experimental results (symbols) for the half-width of the magnetic signature as a function of lift-off.

theoretical values were calculated at two sensor positions corresponding to the primary and secondary fluxgates of the gradiometer and the values were subtracted. Considering the rather crude approximations used in the theoretical model, the agreement between experimental and analytical data for the peak magnetic flux density is surprisingly good.

Another parameter that can be readily used to compare the experimental results is the half-width of the bi-polar magnetic signature, which was defined as half of the lateral separation between the positive and negative peaks. The theoretical curve for the normalized half-width as a function of the normalized lift-off was previously published by author *et al.* [3]. Again, the differential arrangement of the gradiometer slightly complicates the comparison of the experimental data to the theoretical predictions. In the amplitude measurements, we simply subtracted the predicted magnetic field at the location of the secondary sensor from that of the primary sensor to account for the weak, but not entirely negligible secondary signal. Clearly, simple subtraction of the half-widths predicted at the levels of the primary and secondary sensors would not give the right answer, therefore we compared the experimental results simply to the predicted values at the level of the primary sensor. Figure 8 shows our theoretical predictions (semi-solid line) and experimental results (symbols) for the half-width of the magnetic signature as a function of lift-off. There is a good agreement between the theoretical and experimental data except when the normalized lift-off distance exceeds 6.5. It should be mentioned that a large normalized lift-off distance results mainly from a small inclusion diameter, *i.e.*, from the normalization process itself, rather than a large absolute lift-off. Since the peaks are not only smaller but also less sharp in the case of large normalized lift-off distances, it is not surprising that the accuracy of the measured half-width also declines.

Finally, several authors have developed analytical models to predict the magnetic field produced by thermoelectric currents around inclusions of specific geometries such as a cylinder and a sphere respectively in a homogeneous host material under external thermal excitation [9,10]. In subsequent publications, some of these theoretical models were verified by experimental results [2,3]. However, real applications involve more complicated-geometry inclusions. Recently, the author *et. al* have reported that due to the difference in the thermoelectric properties of the host media and the inclusion, the temperature and electric field distributions will be distorted accordingly to the geometry of the inclusion, therefore the thermoelectric signal produced by an inclusion will depend not only on its material properties and size, but also on its shape. The preliminary experimental results indicate that elongated inclusions can be best detected by aligning the externally enforced temperature gradient normal to the major dimension of the inclusion [13]. Further experimental efforts are needed to verify these assumptions and to develop inversion methods capable of quantitatively evaluating the measured magnetic signals in terms of size and shape for inclusions of known physical properties.

5. Conclusions

We conducted an experimental research to verify a developed analytical model based on the magnetic sensing of thermoelectric currents produced by surface-breaking cylindrical tin inclusions embedded in copper under the influence of an external temperature gradient. The diameter of the inclusions and the lift-off distance varied from 4.76 to 12.7 mm and from 1 to 8 mm respectively. A temperature gradient of 1.46°C/cm in the copper specimen was induced. The resulting magnetic flux densities ranged from 60 to 1460 nT was measured by a fluxgate magnetometer. The experimental data obtained in the detection of surface-breaking cylindrical tin inclusions in copper was in good qualitatively agreement with the proposed analiytical model. This paper also presents experimental evidence that illustrated the potential for the non contacting thermoelectric technique to detect and characterize metallic inclusions of different geometries based on their magnetic signature.

Acknowledgment

This work was performed at UMSNH-MEXICO and CENIM-ESPAÑA with funding from CONACYT-MEXICO under project CB-80883.

1. H. Carreon, *J Alloy Compd* **427** (2007) 183.
2. H. Carreon, *NDT & E Int* **39** (2006) 22.
3. H. Carreon, P.B. Nagy, and AH Nayfeh, *J Appl Phys* **88** (2000) 6495.
4. J.H. Hinken and Y. Tavrin, *Rev Progress Quant NDE* **19** (2000) 2085.
5. Y. Tavrin, G.S. Krivoy, and J.H. Hinken, *Rev Progress Quant NDE* **20** (2001) 1710.
6. E. Rodriguez, R. Godinez, and E. Vazquez, *Rev Mex Ing Biomed* **26** (2005) 37.
7. B.A. Auld, J.C. Moulder, *J Nondestr Eval* **18** (1999) 3.
8. Y. Tavrin, M. Siegel and J.H. Hinken, *IEEE Trans Appl Supercond* **9** (1999) 3809.
9. X. Kleber, *NDT & E Int* **41** (2008) 364.
10. P.B. Nagy and A.H. Nayfeh, *J Appl Phys* **87** (2000) 7481.
11. H. Carreon, *Wear* **265** (2008) 255.
12. H. Carreon, S. Barriuso, G. Barrera, J.L. González, and F.G. Caballero, *Surf Coat Technol* **206** (2012) 2942.
13. H. Carreon, *Int. Mech. Eng. Cong. & Exp.* ASME-IMECE2011-62147 **30** (2011) 1.